Astron. Astrophys. 355, 1201–1208 (2000)

ASTRONOMY AND ASTROPHYSICS

Current-driven instabilities in astrophysical jets

Non linear development

T. Lery[1,2]**, H. Baty**[3]**, and S. Appl**[4]

[1] Dublin Institute of Advanced Studies, 5 Merrion Square, Dublin 2, Ireland
[2] Department of Physics, Queen's University, Kingston, Ontario, K7L 3N6, Canada
[3] Observatoire de Strasbourg, 11 rue de l'Université, 67000 Strasbourg, France
[4] Institut für Angewandte Mathematik, Universität Heidelberg, Im Neuenheimer Feld 293, 69120 Heidelberg, Germany

Received 3 November 1999 / Accepted 21 January 2000

Abstract. The non linear development of instabilities driven by the presence of an electric current is investigated for magnetized jets using 3-dimensional MHD simulations. General magnetic equilibria for cold supermagnetosonic jets with constant velocity are considered in order to study the influence of the initial configuration on the non linear evolution. It is found that the current density is redistributed within the inner part of the jet radius with a characteristic time scale and an axial wavelength in agreement with the linear analysis. For equilibria having a pitch profile that increases with radius, an internal helical ribbon with a high current density is forming. It gives rise to considerable dissipation which is radially localized, and may result in heating and particle acceleration within the jet.

Key words: instabilities – magnetic fields – ISM: jets and outflows – galaxies: active – galaxies: jets

1. Introduction

The current consensus on the nature of collimated astrophysical jets from young stellar objects (YSO) and active galactic nuclei (AGN) holds that their magnetic field and associated electric current may play a key role in their structure and dynamics. While there is an exhaustive literature concerning jet launching, collimation and propagation, the stability properties of such current carrying magnetized jets have been investigated only recently.

In a preceding paper (Appl et al. 2000, hereafter paper I), we have addressed the stability of magnetized astrophysical jets with respect to modes driven by the electric current density distribution. These current-driven (CD) instabilities have been suspected to disrupt (Eichler 1993, Lucek & Bell 1996, Spruit et al. 1997) or at least to affect the magnetic structure drastically as the jet propagates (Todo et al. 1993, Begelman 1998). In realistic magnetized jet configurations, magnetohydrodynamic instabilities are generally a mixture of Kelvin-Helmholtz (KH), pressure-driven, and CD modes. The non linear development of KH instabilities in jets has been widely studied in the literature (see for example Hardee et al. 1997, Bodo et al. 1998, Micono et al. 1998), unlike the CD modes.

In paper I, we have performed a linear stability analysis of cold supermagnetosonic jets for a large variety of magnetic configurations. It has been shown that the CD instabilities grow rapidly on time scales of order of the Alfvén crossing time in the jet frame, and they are therefore likely to modify the magnetic structure of the jet. However, they are internal modes since the radial displacement becomes very small at the jet surface as shown by the linear eigenfunctions. This led us to conclude that the CD instabilities would not disrupt the jet.

The aim of the present paper is to investigate the non linear development of CD instabilities for magnetized astrophysical jet. Magnetic configurations representative of the general classes defined in paper I are considered. We carry out numerical computations using a 3-dimensional evolution code issued from laboratory plasma physics (Lerbinger & Luciani 1991, Baty et al. 1993) which was adapted to astrophysical jets. For numerical reasons, we mainly focus on early non linear phases that are quasi-ideal (the resistivity effect being negligible), and we only superficially investigate more resistive later stages.

The paper is organized as follows. Magnetic equilibria assumed for the jet configuration and their stability properties are presented in Sect. 2. The next section is devoted to the numerical procedure and is followed by the results of the non linear simulations. Finally, consequences for jet structure are discussed in Sect. 5, and conclusions are drawn in Sect. 6.

2. Jet equilibria and stability

2.1. Magnetic configurations

Following paper I, we consider an infinitely long cylindrical jet with a radius $r = R$. Cylindrical coordinates (r, ϕ, z) are used. We consider a jet with constant density and velocity, as well as negligible thermal pressure and rotation. This excludes pressure-driven instabilities. The CD instabilities are then easily identified as they are internal modes, and KH ones only arise due to the vortex sheet at the jet boundary. Hence, cold jets with

Send offprint requests to: lery@cp.dias.ie

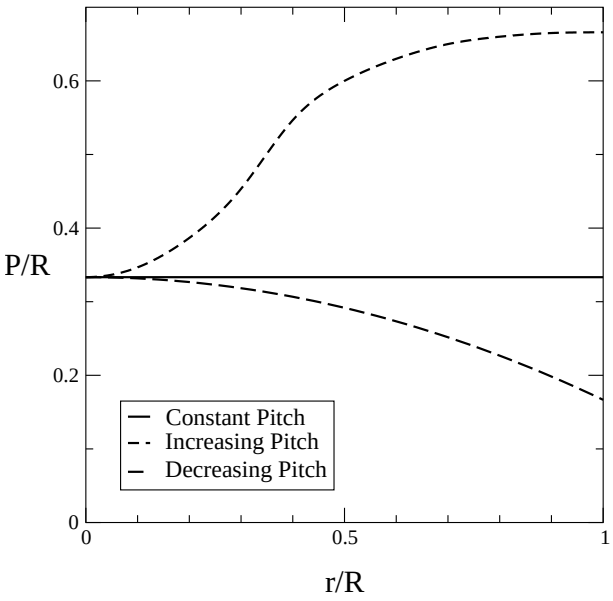

Fig. 1. Variations of the pitch profiles P/R as a function of the radial coordinate r. Solid, dashed and long dashed lines respectively correspond to constant (CP), increasing (IP) and decreasing (DP) pitch profiles.

force-free magnetic field $\boldsymbol{J} \times \boldsymbol{B} = 0$ are retained, $\boldsymbol{J}$ and $\boldsymbol{B}$ being the electric current density and the magnetic field respectively. In the linear phase, at sufficiently high fast-magnetosonic Mach numbers (M larger than unity), the jet boundary becomes effectively rigid for CD modes, and stability properties are similar in the jet frame and for a static configuration bounded by a perfectly conducting wall (See paper I). We conjecture that these results remain true in the non linear regime due to the internal character of CD modes. Hence, the jet dynamics can be modeled by a static configuration bounded by a perfectly conducting wall. Consequently, KH instabilities are excluded from our computations.

In order to cover a wide range in physical conditions, we consider various equilibria as in paper I. We first retain a simple model well studied in other contexts, the *Bessel function model* (BFM) which represents a linear force-free field $\boldsymbol{J} = \alpha \boldsymbol{B}$, with α being a constant. We use the same parameter as in paper I where $\alpha R = 3.832$. Cold magnetized configurations are fully determined by the radial profile of only one function, which can be taken to be the magnetic pitch function $P(r) = rB_z/B_\phi$, where B_z and B_ϕ respectively correspond to the poloidal and the azimuthal components of the magnetic field. Next we consider a *constant pitch* (CP) profile with a value of $P = 1/3R$ which roughly corresponds to the average pitch of the BFM case. The third and fourth equilibria are defined by an *increasing* (IP) and *decreasing* (DP) pitch profile, with positive values for the pitch. More precisely, the DP case is given analytically in paper I by Eq. (5) with $n = 2$ and $C = -1$. The exact radial pitch profile for the IP case has been chosen in order to make computations tractable and has been obtained numerically. In the axial region it follows Eq. (5) from paper I with $n = 4$, $C = 1$ and has been flattened in the outer part with $P(R) \simeq 0.66R$. The central pitch value is still equal to $P(0) = 1/3R$. The variations of the pitch function for these three equilibria are plotted in Fig. 1.

2.2. Linear stability analysis

A global normal mode stability analysis of various unstable magnetic configurations including those considered in the present paper has been carried out in paper I. We recall here the main results. It has been found that the dominant CD instability has an azimuthal mode number $|m| = 1$, with a range of unstable axial wavenumbers k. For example, the BFM configuration is unstable for positive kR values situated in the range $[0, 1.04]$, for $m = 1$, with a maximum growth rate $\gamma_m = .035\ t_a^{-1}$ at $kR = 0.7$. The Alfvén time $t_a = R/V_a$ depends on the Alfvén velocity which is defined by $V_a^2 = B_0^2/(\mu_0 \rho_0)$ with B_0 and ρ_0 being the magnetic field and the density on the magnetic axis. For the other cases (CP, IP, DP), where $m = -1$ is dominant, range of unstable kR values is approximately given by $[0, 3]$. The fastest growing k mode for general magnetic configurations and $P_0 = 1/3R$ exhibits a linear growth rate which is one order of magnitude higher than for the BFM (see Table 1 in paper I).

For the BFM and IP cases, a characteristic feature of the $|m| = 1$ mode is given by its ability to satisfy a resonant condition $\boldsymbol{k} \cdot \boldsymbol{B} = 0$ somewhere in the plasma, where $\boldsymbol{k}$ is the wavevector of the perturbation and $\boldsymbol{B}$ the equilibrium magnetic field. The resulting resonant loci, that also correspond to a vanishing radial component of the magnetic field perturbation, are called resonant surfaces. They are given by the roots of $kP + m = 0$ (See paper I). For example, for the BFM configuration, all unstable k values are resonant in the corresponding interval $r/R = [0.829, 1.]$. These resonances correspond to singularities in the linear MHD equations which are resolved by inertia terms in the vicinity of the singular layers (Goedbloed & Hagebeuk 1972). A given ($|m| = 1, k$) mode is related to a radial displacement with a quasi-rigid shift of the central part of the plasma situated inside the resonant magnetic surface for the mode considered. The linear plasma perturbation gives then an helical distortion of the jet core situated inside the resonant radius, which is close to the jet radius whatever the k value. Similar results are obtained for the IP case, except that the radial displacement is less confined inside the resonant radius (due to inertial effects since the growth rate is one order of magnitude larger) vanishing only at the jet radius. The resonant radius (for the dominant mode) is now located midway between the axis and the jet boundary.

For the CP and DP cases, the most unstable kR values including the fastest growing one are non resonant. Consequently, the radial component of the perturbed magnetic field is non zero everywhere and vanishes only at the outer radial boundary. Moreover, the radial displacement is very similar to the IP case.

Hence, except for the BFM case, the radial displacement is independent of the type of the mode, resonant or not, while the radial component of the magnetic field vanishes exactly at the resonant radius when it exists.

3. The numerical model

The computations of the non linear development of current-driven modes are carried out using the cylindrical evolution code, XTOR (Lerbinger & Luciani 1991). Initially, XTOR was devoted to study the non linear evolution of (ideal and resistive) kink and tearing modes in an axially periodic geometry. Important results using XTOR in tokamak context have been obtained both in cylindrical geometry (Baty et al. 1991) and in toroidal geometry (Baty et al. 1993). In an axially periodic configuration of length L, allowed axial wavenumbers k are given by $k = 2\pi n/L$ (n being an integer). A jet configuration is certainly not periodic in the axial direction, and consequently all the k values must be a priori retained. However, increasing the length means adding more k values in the periodic configuration. From a computational point of view, the maximum k value is only limited by the amount of memory storage. Following the preceding idea, we are able to use a cylindrical version of the periodic code XTOR, with the highest possible length value in order to include the highest possible number of k wavenumbers in the simulations.

3.1. Equations and the numerical scheme

XTOR solves the full set of compressible and dissipative MHD equations, which can be written (in non-dimensional form):

$$\frac{\partial \rho}{\partial t} + \nabla \cdot (\rho \boldsymbol{v}) = 0, \tag{1}$$

$$\rho \left[\frac{\partial \boldsymbol{v}}{\partial t} + \boldsymbol{v} \cdot \nabla \boldsymbol{v} \right] = \boldsymbol{J} \times \boldsymbol{B} - \nabla p + \rho \nu \triangle \boldsymbol{v}, \tag{2}$$

$$\frac{\partial p}{\partial t} + \boldsymbol{v} \cdot \nabla p = -\Gamma p \, \nabla \cdot \boldsymbol{v} \tag{3}$$

$$\frac{\partial \boldsymbol{B}}{\partial t} = \nabla \times (\boldsymbol{v} \times \boldsymbol{B}) - \nabla \times (\eta \boldsymbol{J}), \tag{4}$$

$$\boldsymbol{J} = \nabla \times \boldsymbol{B}. \tag{5}$$

Here, ρ is the mass density, p the plasma pressure, $\boldsymbol{v}$ the fluid velocity. η and ν are the magnetic diffusivity and the kinematic viscosity respectively, and Γ is the ratio of specific heats (a value 5/3 is used). The equations are made dimensionless by setting the jet radius R, the equilibrium density ρ_0, the magnetic field on the axis B_0, as well as μ_0, to unity. The energy equation is as simplified as possible, describing only energy convection (Eq. 3) because the aim of the present simulation is to understand primarily the dynamics. The MHD equations (1-5) are integrated in time using a second order semi-implicit scheme, which allows large time steps limited only by the non linear physical plasma phenomena (Lerbinger & Luciani 1991). Radially, finite differences on two staggered meshes are used. Variables are expanded in double Fourier series in θ and z and operations are performed using fast Fourier transform (FFT). In this study, 100 radial grid points are retained. As concerns the $\theta \times z$ directions, 16×160 and 24×128 grid points are used corresponding then to 5, *i.e.,* $m = 0, \pm 1, \pm 2, \pm 3, \pm 4$, and 8 azimuthal modes (respectively) after de-aliasing (Aydemir & Barnes 1985), each mode with a band of 80 axial wavenumbers centered around the fastest growing one.

3.2. The numerical procedure

To investigate the non linear evolutions of the unstable configurations described previously, we start the simulations by adding small $|m| = 1$ velocity perturbation ($v \approx 10^{-4} V_A$) to the different linearly unstable k wavenumbers of the initial equilibrium. For each k, a random phase is used. Since the CD instabilities are ideal, the linear and the early non linear phases are computed by setting a vanishing resistivity coefficient, *i.e.,* $\eta = 0$ in Eq. 4. After a quasi-linear phase characterized by an almost constant growth rate that is in agreement with the linearly most unstable k value, the non linear regime is followed using an increasing viscosity coefficient in order to resolve small-scale velocity and magnetic field structures (whose dimensions are of the order of the numerical resolution) that can form. It also allows to follow more clearly the possible saturation by dissipating the residual oscillations around a bifurcated equilibrium (see below). Typically, the kinematic viscosity ν varies approximatively from 10^{-5} at the beginning to 10^{-3} at the end of this first stage of the simulation. During the following second stage, a resistivity η and a viscosity coefficient ν, both of the order 10^{-3}, are used in order to follow the ensuing resistive relaxation process. This value of the resistivity is optimal in terms of computational efficiency, without allowing the equilibrium to diffuse too drastically. We recall that the aim of the present work is not the careful study of the relaxation process.

4. The results

4.1. The ideal phase

4.1.1. The BFM case

The CD instabilities have been followed by using two periodic length values $L/R = 44$, and 88. As previously explained, L determines the k values included in simulations via $k = 2\pi n/L$, n being an integer. Therefore, computations retain 7 and 14 kR values in the unstable range $[0, 1.04]$ for $L/R = 44$ and $L/R = 88$ respectively for $m = 1$. Only the $L/R = 88$ results are reported in the present paper since results for the two length values are similar. After a quasi-linear phase characterized by an almost constant growth rate, which approximately corresponds to the linear growth rate of the fastest $(m = 1, k)$ growing mode, $m > 1$ modes are non linearly driven. This is illustrated by Figs. 2 and 3, where the time evolution of kinetic and magnetic energies of the different m modes integrated over all k values are plotted. These figures also show that a quasi-saturated state is attained at the end of this ideal phase *i.e.,* at $t = 650\ t_a$. This state corresponds to constant levels for magnetic energy and oscillations in kinetic energy. We have checked that adding more viscosity, with a final value of $\nu = 10^{-2}$ (instead of $\nu = 10^{-3}$), suppresses these oscillations by dissipating kinetic energy. Viscous relaxation allows to avoid numerical os-

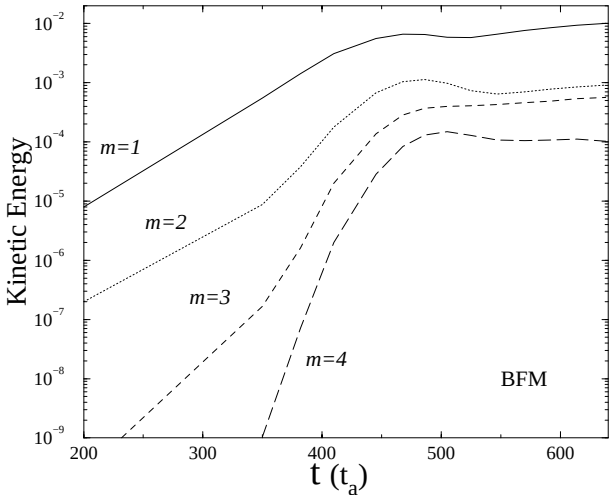

Fig. 2. Kinetic energy for different m modes ($m = 1$ to 4) as function of time for the Bessel force free model (BFM) case during the ideal phase.

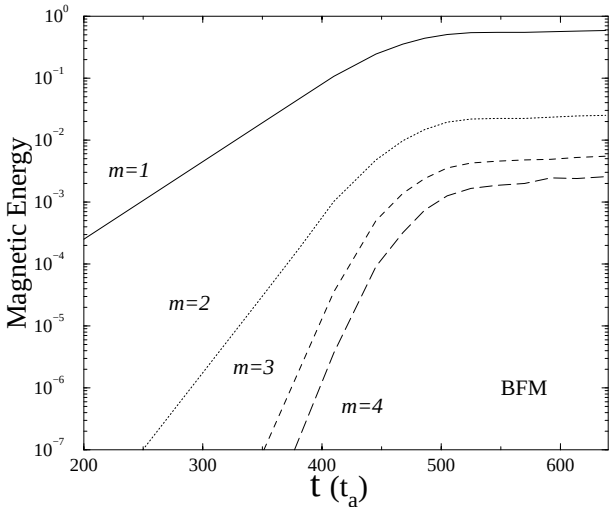

Fig. 3. Magnetic energy for different m modes ($m = 1$ to 4) as function of time for the BFM case during the ideal phase.

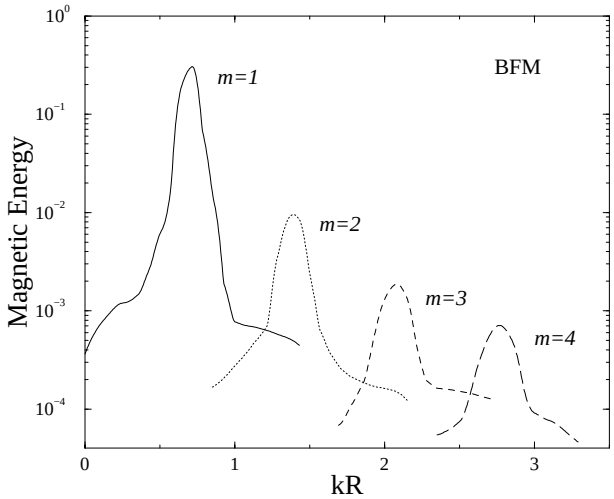

Fig. 4. Magnetic energy for different m modes ($m = 1$ to 4) as a function of the normalized axial wavenumber kR when the BFM configuration is saturated.

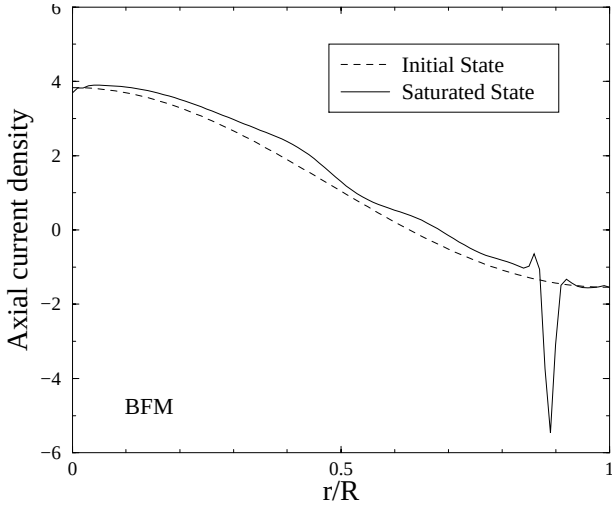

Fig. 5. Radial profile of the axial component of the current density at a given z. The dashed line corresponds to the initial equilibrium while solid line stands for the saturated BFM case. For a given z the azimuthal angle is chosen such that the amplitude of the perturbation is largest.

cillations around the secondary equilibrium. For the saturated state, we have investigated the distribution of magnetic energy among the different k wavenumbers included in the simulation. The results, displayed in Fig. 4, indicate two important features. Firstly, the inclusion of 4 m azimuthal mode numbers in the simulation is sufficient, since the level of the $(m = 4, k)$ modes is very small with respect to the dominant $(m = 1, k)$ ones. Secondly, the saturated state is dominated by the fastest linearly growing $m = 1$ mode, even though the non linearly driven $m = 2$ mode is far from being negligible. The presence of $m > 1$ modes are indeed necessary for the non linear saturation mechanism to be at work through a cascading process towards small length scales. The free magnetic energy is then transferred from the linearly unstable small k wavenumbers (i.e. high axial wavelengths) of $m = 1$ mode towards higher linearly stable k wavenumbers of $m = 2, 3, ..$ modes.

We have also investigated the corresponding magnetic and electric current structures. Our results show the development of a current concentration along the jet configuration, as shown in Fig. 5 for the axial current density. Its maximum is radially localized at the resonance of the linearly dominant mode. In the jet, this concentration takes the form of an helical ribbon of intense negative current superposed on the contribution coming from the initial equilibrium. The helicity corresponds to the pitch of the dominant $(m = 1, k)$ mode. This quasi-singular structure resembles the current sheet found when an internal kink mode ideally saturates in a tokamak (Rosenbluth et al. 1973). However, in this latter periodic configuration, as only one $(m = 1, k_0)$ resonant mode is generally linearly unstable, the non linear harmonics are then given by (m, mk_0). As a consequence, all the non linearly driven modes are resonant at the same radial loca-

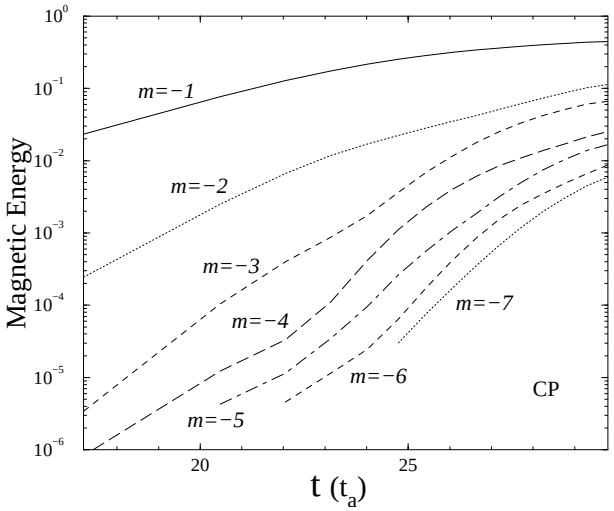

Fig. 6. Magnetic energy for different m modes ($m = -1$ to -7) as a function of time for the constant pitch (CP) case, during the ideal phase.

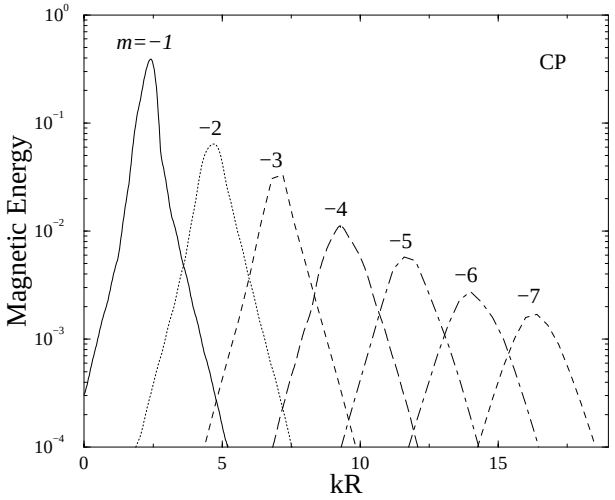

Fig. 7. Magnetic energy of the different m modes ($m = -1$ to -7) as a function of the normalized axial wavenumber kR at the end of the ideal phase for the constant pitch configuration.

tion giving rise there to a discontinuity in the magnetic field and to a singularity in the electric current density. In fact, this situation is not physical and a non-zero resistivity (even very small) is enough to regularize the singularity. In the present jet configuration, a range of $(m = 1, k)$ resonant modes are linearly unstable, and again a wider range of (m, k) modes are consequently driven. Since all these modes resonate at different radial positions, the non linear current structure should be affected by a radial enlargement compared with the tokamak current sheet. However, the radial resonant region $r/R = [0.83, 1]$ is rather limited and therefore the current concentration is little enlarged, as seen in Fig. 5.

4.1.2. The other magnetic configurations

As concerns the non linear development of CD modes (ideal phase) for the three other classes (CP, DP, and IP), again two periodic length values are used, i.e. $L/R = 15.7$ and 31.4 in order to respectively include 7 and 14 kR values for $m = -1$ (most unstable now) in the interval $[0, 3]$ in the simulations. Again, similar results for the two length values have been found, only the larger case ($L/R = 31.4$) is presented here. However, contrary to BFM case, a higher number of azimuthal modes (7 values have been retained) must be included as $m = -2, -3, -4, ..$ modes are linearly unstable (see paper I). The time evolution of the magnetic energy is plotted in Fig. 6 for the CP case and shows that $|m| > 1$ modes are again non linearly driven. However, the saturation is less clear even when a higher viscosity coefficient ν ($\approx 10^{-2}$) is used. The cascading process towards smaller scales probably requires the inclusion of higher $|m|$ and k wavenumber values in this case in order to clearly reach the saturation.

Nevertheless, since the magnetic energy level of the $m = -7$ mode is three orders of magnitude smaller than the $m = -1$ one, the non linear state obtained at the end of this ideal phase, *i.e.*, $t = 30\ t_a$, exhibits the essential features of the non linear ideal state. The repartition of the magnetic energy among the different k wavenumbers included in the simulations has been examined. The corresponding results are plotted in Fig. 7 and show that the non linear state is dominated by the $m = -1$ mode, but with a more important relative contribution of higher $|m|$ modes with respect to the BFM results. Similar results have been found for DP and IP cases.

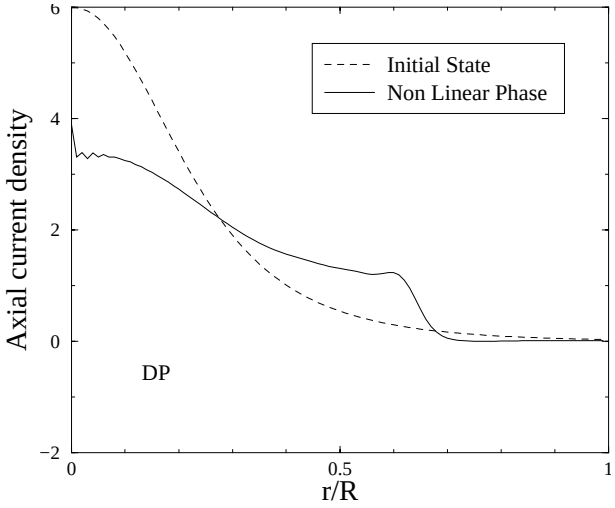

Fig. 8. Radial profile of the axial component of the current density for the DP case at given z and θ at the end of the ideal phase. The dashed line corresponds to the initial equilibrium while solid line stands for the non linear ideal phase configuration.

As concerns the current structure, it has been found that CP and DP configurations only exhibit a weak non linear deformation of current density, as shown in Fig. 8, without the formation of large magnetic gradients (see the intense current concentration for the BFM case for comparison).

This is not the case for the IP configuration, where a strong current concentration non linearly develops as shown in Fig. 9.

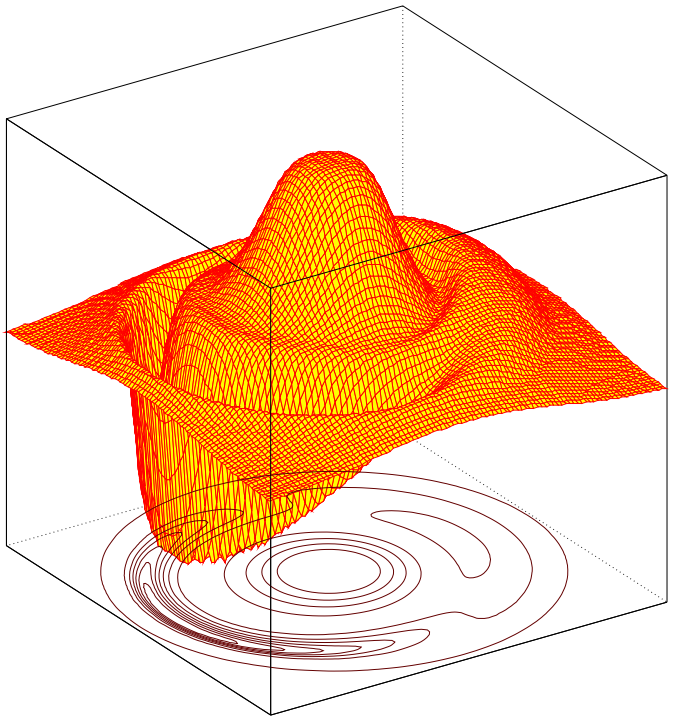

Fig. 9. Spatial variation of the axial component of the current density J_z for the IP case for a section of the jet at the end of the ideal phase. The corresponding contour plots are displayed.

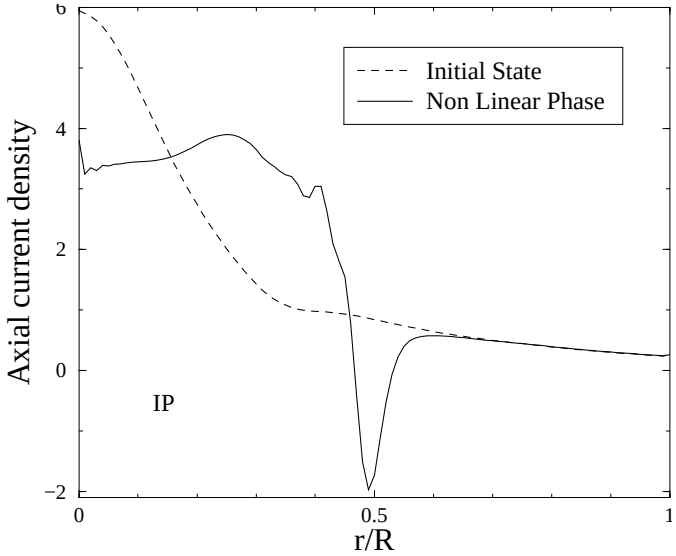

Fig. 10. Radial profile of the axial component of the current density J_z for the IP case at the end of the ideal phase. For a given z the azimuthal angle is chosen such that the amplitude of the perturbation is largest. The dashed line corresponds to the initial equilibrium while solid line stands for the non linear ideal phase configuration.

In this figure that represents the spatial variation of the axial component of the current density J_z in a section of the jet, a negative current sheet appears inside the jet at the resonance of the linearly dominant mode. Indeed the corresponding IP current layer plotted in Fig. 10 at the end of our ideal phase still displays a negative spike similar to the BFM case. However, the current concentration is less peaked than in the BFM case with a broader radial structure.

These results can be explained by the non resonant nature of the dominant CD modes for DP and CP cases, contrary to IP and BFM configurations where the fastest linearly growing mode is resonant. Secondly, it has been found that the different linearly unstable $(m = -1, k)$ modes for IP case resonate everywhere between the axis and the outer limit. The resulting non linear current structure is strongly broadened compared to BFM case. However, it remains an internal structure within the jet.

The preliminary conclusion based on the maximum linear growth rate of the $|m| = 1$ mode to measure the importance of CD instability can be extended by taking the characteristic time scale necessary to reach the non linear ideal state. Indeed, this characteristic time scale, which is of the order of 500 Alfvén time for the BFM case, is approximately 30 for the other unstable magnetic configurations with a pitch value around $1/3R$.

4.2. The relaxation process

An important point concerns the ensuing relaxation process. Indeed, small scale magnetic structures as obtained in BMF and IP cases would certainly lead to non negligible diffusion in presence of a non-zero small resistivity. For example, in a periodic tokamak configuration, the effect of the resistivity is to lead to the diffusion of the singular current sheet that is forming in the limit of vanishing viscosity, to some non-zero finite thickness current concentration determined by the resistivity value. The ensuing process takes the form of a stationary magnetic reconnection, with a magnetic island growing in the plasma core. The time scale of the process is intermediate between the Alfvén and the resistive ones (Kadomtsev 1975). The relaxation process stops when the configuration has reached a stable state of lower magnetic energy which was inaccessible in ideal MHD.

In order to follow the instability further, a numerical resistivity has been applied in cases where intense magnetic gradients are formed (IP and BFM cases). The resistivity has been turned on at the end of the previous ideal phase when the smallest magnetic scale approaches the grid resolution. It corresponds in time to $t = 650\ t_a$ for the BFM case and to $t = 30\ t_a$ for the three other configurations. An optimal value $\eta = 10^{-3}$ has been used. Higher resistivity values would lead to unrealistic dissipation of the whole configuration and smaller ones would be prohibitively time consuming. Unfortunately, due to computational limitations, it was not possible to fully reach the relaxed state with the resistivity we have been using. This is mainly due to the increase with time of the number of modes driven to high amplitudes. It corresponds in our code to a drastic reduction of the time step, preventing us from following instabilities on long time scales. The memory storage limits have also prevented us from a further increase in the number of modes.

The previous effect can be explained by the increase of the number of linearly unstable modes. Indeed, a non zero resistivity triggers the development of purely resistive tearing-like modes which were ideally stable. This drives an efficient coupling be-

tween various (ideal and resistive) modes. A large number of modes are consequently non linearly driven, leading to a state that corresponds to the beginning of the turbulent cascade. A process similar to the one observed here and called the dynamo action is observed in the RFP, and can be described in terms of turbulent relaxation (Taylor 1986, Biskamp 1996). The efficiency of the coupling between nonlinearly interacting modes depends on the resistivity value (Nordlund & Mazur 1994). In the present work, a rather high resistivity value compared to the expected one is employed mainly for computational reasons leading probably to a too efficient coupling. Nevertheless, we can conclude that one expects a strong localized (radially) dissipation when the magnetic structure of the jet is given by a globally increasing pitch.

5. Astrophysical consequences

It has been shown that non linear instabilities develop on rapid time scales and therefore should affect internal magnetic structures. This is not the case for the BFM configuration that corresponds to a very particular equilibrium of minimal magnetic energy which has been used for illustration purposes (see paper I). When a current sheet forms *i.e.,* in the IP case, a kinked inner tube should appear due to helical distortion. Reconnection and turbulence in such a configuration are likely to occur and could accelerate particles in the vicinity of this surface. The ensuing saturated configurations may look like a hollow tube as observed in some jets. As has been shown in the previous section, this state of developing turbulence should have its origin in a strong coupling between different ideal and resistive modes. We have conjectured that this turbulent phase indicates that the system would further undergo a relaxation process. Unfortunately, we have not been able to explore more deeply this question, because of the limited resolution in our calculation. However, we can conclude that jets with increasing pitch profiles should give rise to important dissipation, acceleration of non-thermal particles, and relaxation towards a state of lower magnetic energy.

Also, the turbulent state can probably lead to a local dissipation of energy and therefore to heating along the current layers within the jet core. Hence the magnetic instabilities could be at the origin of an heating mechanism in jets. This may help understand some YSO jets observations where the local temperature decreases more slowly than expected, or where temperature increases are not followed by analogous increases in density close to the source (e.g. at about 200 AU, Bacciotti and Eislöffel 1999). Such a localized current is not observed if the unstable modes are non resonant (CP and DP cases). Internal helical features in jets can therefore arise as a consequence of current-driven instabilities depending on whether their magnetic structure possess a radially increasing or decreasing profile.

The magnetic equilibria used in the present study are similar to realistic jet models. As an illustrative case, comparisons can be made with the Given Geometry model (Lery et al. 1998, 1999, Lery & Frank 2000), that has been recently proposed for outflows from rotating magnetized objects confined by a uniform external pressure. The variations of the magnetic field where the jet becomes cylindrical and the corresponding pitch can be derived. With this model, pressure and velocity gradients are present contrary to the present work. However, it is found that the model produces various types of pitch profiles that can always be classified following the general types shown in the present study, *i.e.,* with increasing, constant and decreasing pitch. The most realistic angular velocity profiles, *i.e.,* with Keplerian rotations, give rise to increasing pitch profiles. This is precisely the kind of magnetic profile which develops helical current sheets.

Finally, our results have bearing on the integrity of the MHD jets. The perturbation associated with the CD instabilities remain confined to the inner parts of the jet also in the non linear regime. We therefore conclude that the CD modes also non linearly are internal instabilities which will not lead to a destruction of the jet, but only to a modification of the magnetic structure. This is in good agreement with Todo et al. (1993) and Begelman (1998). Our work also supports the 3D jet stability study by Rosen et al. (1999) who have found that the jet is more dissipative and less easily disrupted for important azimuthal magnetic field configurations. Therefore, nothing in our results indicate a possible disruption of the jet by the CD instabilities as suggested by Eichler (1993), Lucek & Bell (1996) or Spruit et al. (1997).

6. Conclusions

The subject of the present paper is the nonlinear evolution of current-driven MHD instabilities in astrophysical jets. Since the precise magnetic structure of jet configurations is not known presently, various equilibria characterized by their magnetic pitch and previously studied in the linear regime have been investigated. In particular, these are configurations with a constant pitch (CP), with radially increasing (IP) and radially decreasing pitch (DP), and a linear force-free field (BFM). The BFM case represents a very particular equilibrium of minimum magnetic energy that has merely served for illustration purposes, since its evolution can be followed over longer time scales. A 3D evolution MHD code for cylindrical equilibria of fusion plasma XTOR has been adapted and applied to astrophysical jet configuration. We are mainly interested in the current-driven instabilities, that are suspected to change drastically the jet structure.

An important result is that the dominant unstable modes are those which possess the fastest linear growth rate in the nonlinear regime. This implies that a linear analysis well predicts the characteristic time scale to obtain a non linear state and the axial wavelength of the resulting deformation. This is true even when the instability has grown to a large amplitude. Unstable modes can either be resonant or not, according to whether the equilibrium contains a resonant magnetic surface or not. Both resonant and non resonant modes show a similar (linear) helical radial displacement of the inner parts of the plasma column and the axial electric current distribution adjusts itself within this region. The initially more centrally peaked current is redistributed within the inner part as the instability develops non linearly, while the outer parts remain unaffected. It is found

that equilibria which contain a resonant surface (IP and BFM cases), non linearly develop a negative current spike at the resonant radius. The perturbed configuration has the form of an internal helical ribbon with a high current density, which may give rise to an important dissipation. Ultimately, this probably leads to the heating of the jet plasma or to the acceleration of non-thermal particles.

The results presented in this work are valid for magnetic configurations where the jet velocity is constant. This was done in order to spatially separate KH and CD modes, and to focus only on the effects of the later ones. However, in more realistic jets, the velocity gradients should cause coupling between these instabilities. Moreover, pressure gradients could give rise to sausage type ($m = 0$) instabilities which could play a role in the knotty aspect of jets. We plan to study these effects in a future study.

Acknowledgements. We thank the anonymous referee for his remarks. The numerical calculations were performed on the CRAY C98 at I.D.R.I.S., Orsay (France). T.L. acknowledges support from the NSF Grant AST-0978765. S.A. has been supported by the Deutsche Forschungsgemeinschaft (SFB 359).

References

Appl S., Lery T., Baty H., 2000, A&A, in press (paper I)
Aydemir A.Y., Barnes D.C., 1985, J. Comput. Phys. 59, 108
Bacciotti F., Eislöffel J., 1999, A&A 342, 717
Baty H., Luciani J.F., Bussac M.N., 1991, Nuclear Fusion 31, 2055
Baty H., Luciani J.F., Bussac M.N., 1993, Phys. Fluids B 5, 1213
Begelman M.C., 1998, ApJ 493, 291
Biskamp D., 1996, Ap&SS 242, 165
Bodo G., Rossi P., Massaglia S., et al., 1998, A&A 333, 1117
Eichler D., 1993, ApJ 419, 111
Goedbloed J.P., Hagebeuk H.J.L., 1972, Phys. Fluids 15, No. 6, 1090
Hardee P.E., Clarke D.A., Rosen A., ApJ 1997, 485, 533
Kadomtsev B.B., 1975, Sov. J. Plasma Phys. 1, 389
Lerbinger K., Luciani, 1991, J. Comput. Phys. 97, 444
Lery T., Frank A., 2000, ApJ, in press
Lery T., Heyvaerts J., Appl S., Norman C.A., 1998, A&A 337, 603
Lery T., Heyvaerts J., Appl S., Norman C.A., 1999, A&A 347, 1055
Lucek S.G., Bell A.R., 1996, MNRAS 281, 245
Micono M., Massaglia S., Bodo G., Rossi P., Ferrari A., 1998, A&A 333, 989
Nordlund P., Mazur S., 1994, Phys. Plasmas 1, 4032
Rosen A., Hardee P.E., Clarke D.A., Johnson A., 1999, ApJ 510, 136
Rosenbluth M.N., Dagazian R.Y., Rutherford P.H., 1973, Phys. Fluids 16, 1894
Spruit H.C., Foglizzo T., Stehle R., 1997, MNRAS 288, 333
Taylor J.B., 1986, Rev. Mod. Phys. 58, 741
Todo Y., Uchida Y., Sato T., Rosner R., 1993, ApJ 403, 164